ACS APPLIED NANO MATERIALS

www.acsanm.org Article

ZSM-5 Zeolite Nanosheet-Based Membranes on Porous Polyvinylidene Fluoride for High-Flux Desalination

Zishu Cao, Landysh Iskhakova, Xinhui Sun, Zhong Tang, and Junhang Dong*

Cite This: *ACS Appl. Nano Mater.* 2021, 4, 2895−2902 Read Online

ACCESS | Metrics & More | Article Recommendations | Supporting Information

ABSTRACT: A submicrometer-thick molecular sieve zeolite nanosheet laminated (ZNL) membrane has been synthesized on macroporous polyvinylidene fluoride (PVDF) substrate via the simplistic vacuum filtration-coating method. The membrane has been demonstrated with extraordinary water flux (~11 kg/m^2·h) and salt rejection (~99.9%) in pervaporation (PV) desalination of a multicomponent brine with 22 wt % of total dissolved salts (TDS) including Li^+, Na^+, K^+, Mg^{2+}, Cl^-, and SO_4^{2-}, etc. The desalination of high-salinity brines is critical to treatment and beneficial use of many industrial produced waters. The large aspect ratios (>100) and preferable *b*-orientation of the densely layered nanosheets make the solution dewatering rate surpass the ion diffusion rates in the nanoscale internanosheet spaces. This unique transport behavior effectively prevents the dissolved salts from migrating through the ZNL layer and stabilizes the water flux and ion rejection rates. The supported multilayered ZNL membrane, which is interlocked by the substrate-type PVDF binder, exhibits structure and performance stability in PV desalination of high-TDS brines.

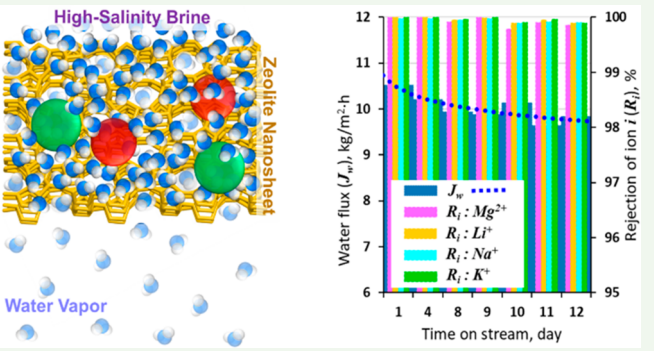

KEYWORDS: *zeolite, nanosheets, membrane, polymer substrate, desalination*

1. INTRODUCTION

Two-dimensional (2D) crystalline materials, both porous, such as zeolites, metal organic frameworks (MOF), and perforated graphene, and nonporous, such as nonperforated graphene oxides (GO) and molybdenum disulfide (MoS_2), etc., are new types of building blocks for high-efficiency molecular and ionic separation membranes.[1−9] In zeolite nanosheet (ZN) membrane development, the literature works have been so far focused primarily on the MFI-type zeolites. The MFI-type zeolites, especially their alumina-containing ZSM-5 group, are particularly useful for membranes for brine desalination and proton-selective ion conduction because of their exceptional thermal and chemical stabilities, surface ionicity and hydrophilicity, and pore size ideal for water permeation while excluding hydrated ions.[10−13]

The MFI-zeolite crystals possess a three-dimensional channel network. The interconnected channels have cross-sections defined by 10-membered rings. This channel system consists of nearly cylindrical straight channels (0.56 nm × 0.53 nm) extending along the *b*-axis and channels of slightly elliptical shape (0.55 nm × 0.51 nm) laying zigzag in the *a*−*c* plane (Figure S1). These pore openings are slightly smaller than the kinetic diameters (d_k) of hydrated metal ions and common anions in aqueous solutions (d_k > 0.6 nm) but are much bigger than the d_k value of water (~0.27 nm). Because the ion hydration numbers and hence the hydrated ion kinetic sizes are insensitive to the solution concentration and temperature, defect-free MFI zeolite membranes are particularly promising for ion-sieving desalination of highly concentrated brines. High-salinity brines are a current challenge in the treatment and reclamation of many industrial wastewaters. The existing technologies such as the multieffect flash (MEF) and membrane reverse osmosis (OR) processes are inefficient for desalination of brines with high levels of total dissolved salts (TDS).[14−18]

In the past decade, nanometer-thick pure-silica MFI zeolite (i.e., silicalite) nanosheets have been synthesized with the *b*-axis straight channels oriented in the out-of-plane direction (*b*-oriented). The *b*-oriented nanosheets are desirable for molecular transport through the straight channels because of their larger diameter and shorter length.[10,19] The 2D silicalite nanosheets have been used to fabricate continuous MFI membranes on porous ceramic supports by secondary growth of precoated zeolite nanosheet (ZN) seed layers and subsequent thermal activation.[19−21] The obtained silicalite

Received: January 7, 2021
Accepted: March 1, 2021
Published: March 5, 2021

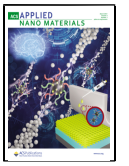

https://dx.doi.org/10.1021/acsanm.1c00046
ACS Appl. Nano Mater. 2021, 4, 2895−2902

nanosheet membranes are *b*-oriented and ultrathin to simultaneously reduce nonselective intercrystalline boundaries and transport resistance.[22] Thus, the MFI nanosheet membrane can overcome the main deficiencies of its conventional membrane structures containing randomly oriented isotropic crystallites. However, these ceramic supported zeolite nanosheet membranes are presently difficult to scale up and expected to be cost-prohibitive. From the practical standpoint, it is highly desirable to fabricate the ZN laminated (ZNL) membranes on low-cost polymer supports. However, the synthesis of ZNL membranes on polymer supports has been hindered by challenges in preparing suspensions of preactivated ZNs and creating strong interconnections between the ZNs and the polymer supports.

Zhang et al.[23] prepared an aqueous suspension of exfoliated silicalite ZNs of which the long-chain C_{22-6-6} biammonium structure directing agent (SDA) was decomposed in piranha solutions through a rather sophisticated procedure. This aqueous suspension of activated ZNs was used to form a ZNL membrane on porous polybenzimidazole by filtration coating. The resultant silicalite ZNL membrane, without binder or secondary growth consolidation, exhibited molecular sieving capability in *n*-/*i*-butane gas permeation. However, such simply stacked ZNL membranes are not applicable to saline water desalination due to the lack of inter-ZN and ZNL-polymer binding to resist ZN interlayer dissociation under surface solvation.[8,23] Moreover, the hydrophobic silicalite exhibits significantly smaller water permeability than does the ZSM-5 zeolite because the latter has a highly hydrophilic surface that dramatically lowers the transport resistance at the pore entrances and enhances intrapore water uptake.[24−28]

Recently, we synthesized *b*-oriented ZSM-5 nanosheets with adjustable framework aluminum contents. The ZSM-5 ZNs were used to fabricate ultrathin (<500 nm) ZNL membranes on porous α-alumina substrates. The ZSM-5 ZNL membrane was synthesized by dip-coating of a nonactivated ZN layer followed by vapor-phase crystallization to firmly bond the ZN layer on substrate.[8] This *b*-oriented ZSM-5 ZNL thin membrane was thermally activated. It displayed a combination of high water flux and salt rejection rates (>99%) in pervaporation (PV) desalination of brines containing 24 wt % of NaCl. The thermally driven PV desalination by porous membranes is theoretically capable of avoiding diffusive transport of the nonvolatile salts into the vapor product and is therefore considered most useful for treating high-TDS brines. However, the dissolved salts can migrate through the liquid-filled nonzeolitic pores to precipitate and block pores in the permeate side. Thus, the conventional MFI zeolite membranes were found to exhibit small water flux because of the long intracrystalline diffusion pathways and low salt rejection rates caused by the large amount of shortcutting intercrystalline salt passages.[8,24,27,29] The ability of the ZSM-5 ZNL membrane to be used for PV desalination of extreme TDS solutions comes from the very fast water diffusion through the straight channels of nanometer-thick individual ZNs. Thus, the water permeation rate surpasses the ion diffusion rates through the nanoscale inter-ZN slits that consequently prevents the dissolved salts from migrating to the permeate side.[8,13] However, the generally small porosity and large thickness of the ceramic supports severely limit the water flux enhancements, and the membrane fabrication processes are complex and energy- and cost-intensive. These drawbacks are serious hurdles to industrial considerations of the inorganic-supported ZNL membranes.

Here, we report the synthesis of ZSM-5 ZNL membranes on the industrially meaningful porous polyvinylidene fluoride (PVDF) substrates by the filtration-deposition method (Figure 1). The polymeric substrates do not allow high-temperature

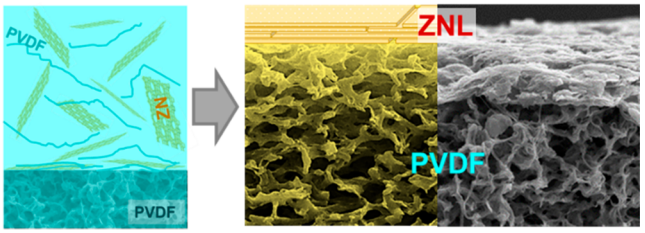

Figure 1. Schematic showing filtration-coating of ZNL membrane on PVDF using PVDF as a binder for ion-sieving desalination.

treatments for removing the SDA and consolidating the ZNL layer via interfacial sintering. We form the membrane of multilayer ZNs on the porous PVDF by vacuum-filtration of a suspension containing ZSM-5 ZNs preactivated by conventional calcination. The direct formation of preactivated and solution-resistant ZNL membrane on the polymer is realized by using a minimal amount of PVDF binder, which is identical to the substrate type. The sparsely networked PVDF binders physically interlock the ZNs to the substrate without seriously masking the zeolitic pore entrances and widening the inter-ZN spaces. The membrane, as compared to the reported zeolite-based membranes (Table S1), has shown extraordinary water fluxes with near-absolute salt rejections in PV desalination of high-TDS brines. The desalination of high-salinity brines is critical to the treatment and beneficial use of many industrially produced wastewaters.

2. EXPERIMENTAL DETAILS

2.1. ZSM-5 Nanosheet Syntheses. The ZSM-5 ZNs were synthesized by a seeded secondary growth method via hydrothermal reactions. The homemade bis-1,5(tripropyl ammonium) pentamethylene diiodide (dC5) was used as SDA. The secondary growth of ZSM-5 ZNs was accomplished by a two-stage hydrothermal reaction process. The first stage was growth of silicalite ZNs from the silicalite nanoparticle seeds, which followed the protocol reported by Jeon et al.,[19] and the second stage was growing a ZSM-5 surface on the silicalite ZN by injecting a controlled amount of aluminum source ($NaAlO_2$) into the reactor. The reaction was uninterrupted between the two stages. The detailed dC5 and ZSM-5 ZN synthesis procedures have been described in the literature and briefly explained in the Supporting Information.[8,19] The as-synthesized ZSM-5 zeolite crystals were rhombus-shaped sheets of micrometer-scale diagonal dimensions. Each rhombus sheet consisted of a tall center core and an encircling uniform flat sheet of nanometer-thickness. The rhombus ZSM-5 crystal sheets were intensively sonicated with 4 mm-diameter zirconia milling beads in aqueous medium to break up the flat sheets from the center cores. The irregularly shaped flat sheet fragments were then separated from the large core particles by the traditional sedimentation-fractionation technique. The uniform nanosheets were then dried and calcined at 500 °C in air for 8 h to remove the SDA.

2.2. Preparation of ZNL Membranes. The ZSM-5 ZNL membrane was coated on the commercially obtained hydrophilic porous PVDF film. The PVDF film was 125 μm-thick with an effective pore size of ~0.45 μm (manufacturer data) and porosity (ε_{PVDF}) of ~80% (Figure S2a and b). This macropore PVDF sheet exhibited a water vapor permeance of 2.16×10^{-3} mol/m^2·s·Pa. The PVDF substrate was also confirmed to be nonswelling after being

https://dx.doi.org/10.1021/acsanm.1c00046
ACS Appl. Nano Mater. 2021, 4, 2895−2902

boiled and then immersed in water for 10 days. The thermally activated ZSM-5 ZNs were dispersed in ethanol via stirring and then intensive sonication for ~8 h. The suspension was placed statically for 40 min to sediment the undispersed ZN aggregates formed during the firing process. The upper portion of the suspension (about 70% of the total liquid volume) was then taken and used for preparing the suspension for membrane coating. The remaining bottom part of the suspension and deposits was dried and quantified to determine the solid contents in the suspensions.

The ZSM-5 ZNs were coated onto the surface of a 3.4 cm-diameter PVDF sheet (i.e., coating area of 9.1 cm^2) via complete filtration of a 3 mL ZN suspension assisted by downstream vacuuming. The ZN suspension for ZNL membrane coating contained 0.02 wt % activated ZSM-5 ZNs and 0.06 wt % of dissolved PVDF in an ethanol (EtOH) and dimethyl sulfoxide (DMSO) mixed solvent. The mixed solvent had an EtOH/DMSO weight ratio of 2:1. Because PVDF is insoluble in water and ethanol but readily dissolves in DMSO, the EtOH/DMSO mixed solvent was used to obtain the dilute solution of PVDF, which was used as the binder for the ZNL membrane. Most of the dissolved PVDF in the coating suspension left with the filtrate liquid, and only a small portion of the PVDF remained in the deposited film to sparsely interlock the ZNs and bond the ZNL layer with the PVDF substrate. The minimal amount of PVDF is expected to avoid excessively covering the ZN surface or enlarging the inter-ZN spacing. The 2:1 EtOH/DMSO weight ratio was experimentally determined to avoid destructive dissolution of the PVDF porous surface (Figure S2c–e) during the filtration coating process while ensuring sufficient dilution of the PVDF binder.

After being coated by vacuum filtration, the PVDF-supported ZNL membrane (ZNL-PVDF) was dried in a vacuum oven at 80 °C for 3 h under an absolute pressure of <1.5 kPa, which is well below the DMSO saturation vapor pressure.[30] The dried membrane was subsequently treated by a 3-h curing period at 120 °C when the oven was maintained at an absolute pressure of ~24 kPa. A ZSM-5 ZNL membrane was also fabricated on a 1.2 mm-thick and 2.5 cm-diameter α-alumina disc with pore size and porosity ($\varepsilon_{alumina}$) of ~0.1 μm and ~30%, respectively. This alumina-supported ZNL membrane (ZNL-alumina) was a replicate of our earlier work for comparison with the ZNL-PVDF (Supporting Information).[8] The bare alumina substrate, because of its smaller porosity and pore size and larger thickness, had a water vapor permeance of 3.15×10^{-5} mol/m^2·s·Pa, which was lower than that of the hydrophilic PVDF by nearly 2 orders of magnitude.

2.3. Membrane Characterizations. The morphological properties and microstructures of the ZNL membranes were examined by scanning electron microscopy (SEM) and energy dispersive X-ray spectroscopy (EDS) using a FEI Scios DualBeam microscope equipped with Ametek Octane Super EDAX. The thicknesses of individual ZN were probed by a Veeco Dimension 3100 atomic force microscope (AFM) using height imaging/profiling under tapping mode. The crystalline phase and orientation of the individual ZN and the supported ZNL membranes were characterized by X-ray diffraction (XRD) using the PANalytical X'Pert Pro diffractometer with Cu Kα radiation (λ = 1.5406 Å) and confirmed by transmission electron microscopy (TEM) observation using a JEOL 2010F field emission electron microscope. The XRD peak identification and crystal phase determination were based upon the standard spectrum of ZSM-5 zeolite powders.[31]

2.4. Membrane PV Measurement and Performance Analysis. The membrane PV desalination experiments were carried out by an apparatus shown in Figure S3 with basic information on permeate sample collection and analysis error determination. The disc-shaped membrane had an active membrane area of 2.5 cm^2 when mounted in the Teflon permeation cell. The feed liquid was continuously circulated. The PV desalination tests were performed for two feed solutions: the first was a 6.77 wt % TDS solution containing 0.20 wt % $MgSO_4$, 6.35 wt % NaCl, 0.19 wt % KCl, and 0.03 wt % LiCl; and the second was a 22.04 wt % TDS solution containing 1.98 wt % $MgSO_4$, 19.06 wt % NaCl, 0.76 wt % KCl, and 0.24 wt % LiCl. These solution compositions are relevant to the reclamation and lithium enrichment from drilling, mining, and CO_2-geostorage generated wastewaters.[18,32] The feed brine flowed over the surface of the ZNL membrane at a volumetric flow rate of 63 cm^3/min, and a N_2 gas stream was used to sweep the substrate surface in permeate side at a flow rate of ~250 STP cm^3/min under ambient pressure. The membrane PV operations were conducted at a temperature of 73 ± 2 °C. The permeate water vapor was collected by condensation in a cold trap immersed in ice–water (0 °C) and analyzed by inductively coupled plasma-mass spectrometry (Agilent 8800 ICP-QQQ) to determine the metal ion concentrations.

The performance of membrane PV desalination is assessed by measuring the water flux (J_w, kg/m^2·h) and ion rejection rates (R_i), which are defined by eqs 1 and 2, respectively.

$$J_w = \frac{Q_w}{A_m} \tag{1}$$

$$R_i = \frac{C_{i,f} - C_{i,p}}{C_{i,f}} \tag{2}$$

where Q_w is the water flow rate through the membrane (kg/h), A_m is the active membrane area (m^2), and $C_{i,f}$ and $C_{i,p}$ (mol/m^3) are the ion concentrations in the feed solution and permeate water, respectively. For the ZNL/substrate two-layer structure, the resistors-in-series model, as expressed by eq 3, applies to correlating J_w with the water vapor permeance (P_m, mol/m^2·Pa·s) and permeability (P_b, mol/m·Pa·s) of each layer.[33]

$$J_w = \frac{P_f^v - P_p^v}{\delta_z/P_{b,z} + \delta_s/P_{b,s}} \tag{3}$$

where P_f^v and P_p^v are the water vapor pressures on the feed and permeate sides, respectively; $P_{b,s}$ and $P_{b,z}$ are the permeabilities of the substrate and the ZNL layer, respectively; and δ_s and δ_z are the thicknesses of the substrate and ZNL layer, respectively. The parametric definition and derivation of the equation are detailed in the Supporting Information. The feed side saturation pressure P_f^v is estimated by the Raoult's law and Antoine equations. The water vapor partial pressure on the permeate side P_p^v is calculated from the water flow rate (Q_w) and the sweep gas flow rate under atmospheric pressure (~1.013 bar). Equation 4 relates the overall P_m of the membrane with the permeances of the ZNL layer ($P_{m,z}$) and substrate ($P_{m,s}$).

$$P_m = \frac{P_{m,s} \cdot P_{m,z}}{P_{m,s} + P_{m,z}} = \frac{1}{\delta_z/P_{b,z} + \delta_s/P_{b,s}} \tag{4}$$

3. RESULTS AND DISCUSSION

3.1. ZSM-5 Nanosheets. The ZSM-5 zeolite crystal obtained by the uninterrupted two-stage hydrothermal secondary growth was rhombus shaped with diagonal dimensions of around 2.0 ± 0.3 μm × 3.0 ± 0.5 μm. Each rhombus crystal consisted of a seed-evolved oval core of 0.3–0.5 μm in length and ~130 nm in height and a surrounding flat fringe area (Figure 2A). The flat flakes fragmentated by sonication had irregular shapes with typical literal dimensions of ~0.7 μm × 1.0 μm and a uniform thickness of ~7.5 nm (Figure 2B and C). The TEM electron diffraction examination revealed an (020) diffraction pattern (out-of-plane b-orientation), and EDS analysis indicated an overall Si/Al ratio of 30 ± 2 for the nanosheets (Figure 2D).

3.2. Supported ZSM-5 ZNL Membranes. The cross-section and surface SEM images of the ZNL-PVDF and ZNL-alumina membranes are displayed in Figure 3A–D. On both substrates, the ZNL membrane layers were free of pinholes and in uniform thicknesses (δ). On the basis of an SEM survey at multiple random locations, the thickness δ of the ZNL layer

https://dx.doi.org/10.1021/acsanm.1c00046
ACS Appl. Nano Mater. 2021, 4, 2895–2902

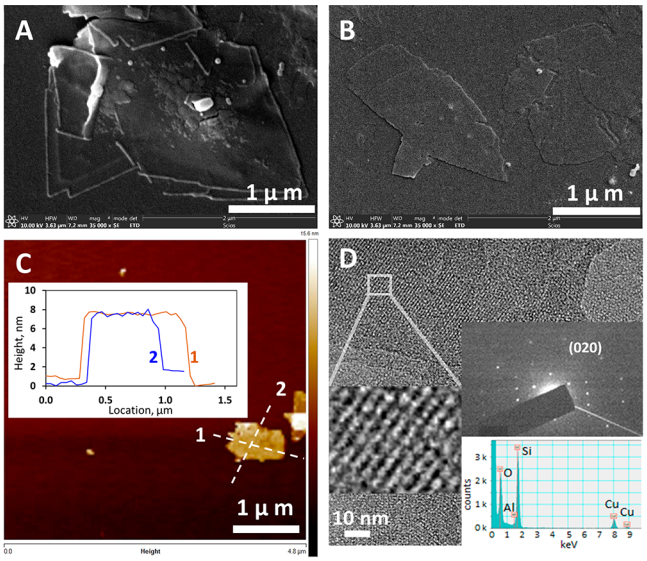

Figure 2. Characterizations of the ZSM-5 nanosheets: (A) SEM image of a typical rhombus-shaped ZSM-5 crystal obtained from the two-stage secondary growth process; (B) SEM image of the fragmentated ZSM-5 nanosheets; (C) AFM tapping mode image of a 7.5 nm-thick nanosheet fragment on silicon wafer; and (D) TEM image of the ZSM-5 nanosheet together with the electron diffraction pattern and EDS spectrum (high magnification TEM inset shows lattice in *b*-axis projection; the total inset image width is 5 nm).

was ~650 nm on the PVDF and ~350 nm on the alumina. The cross-sections of both ZNL layers exhibited dense textures in high-resolution SEM pictures (Figure 3A and C) that were not achieved in coatings without binders on the PVDF or without vapor phase crystallization on the alumina disc (Figure S4). The SEM-EDS line scan results shown in Figure 3E displayed elemental distributions along the ZNL-PVDF membrane depth. The elemental distributions reflected the structure of a PVDF molecule-interlocked ZNL layer on the highly porous PVDF substrate. The presence of C and F in the ZNL top layer evidenced the incorporation of PVDF molecules into the ZN layers. Although the pore dimensions of the PVDF appeared to be much larger than the manufacturer-stated value of 0.45 μm (Figures 3A and S2a and b), penetration of small ZN fragments into the substrate porosity was not observed. The results of XRD examinations in Figure 3F further confirm that the zeolite nanosheets were of pure MFI crystal phase according to the exact match between the XRD spectra of the randomly packed ZNs and the standard powders. The 7.5 nm nanosheet thickness was in the *b*-axis cell direction as confirmed by the sole peak detected at (020) for the ZN lamina deposited on a glass chip. The constituting ZNs in the ZNL layers on both substrates were oriented preferably with the *b*-direction straight channels aligned perpendicular to the surface.

3.3. PV Desalination on ZNL-PVDF. The 0.56 nm × 0.53 nm ZSM-5 zeolitic pore openings are inaccessible to the hydrated metal ions ($M^{m+}\cdot(H_2O)_{nh}$; $M^{m+} = Mg^{2+}$, Li^+, Na^+, and K^+) and anions (Cl^- and SO_4^{2-}), which have kinetic diameters d_k > 0.6 nm.[34,35] Thus, a perfect ZSM-5 membrane, that is, single crystal, is expected to exhibit total rejection of the dissolved salts and good permeability for the small water molecules ($d_k \approx 0.27$ nm). The ZNL-PVDF achieved nearly perfect ion rejection rates (R_i > 99.9%) even for the feed with TDS of 22.04 wt % (Figure 4A) because the ion hydration number "nh" and kinetic sizes are insensitive to salt concentration and solution temperature.[36,37] It is remarkable that the ZNL-PVDF reached or even exceeded the ion rejection rates of the ZNL-alumina, although the latter was densified by vapor phase crystallization and consolidated by high temperature calcination. This indicates that the PVDF-bound ZNL layer also has effectively prevented the dissolved salts from transporting through the inter-ZN pathways. The prevention of salt migration through the multilayer ZNL membrane for the extremely high TDS feeds relies on the ultrafast water permeation through the nanometer-length straight channels of single ZNs. The rate of water removal from the inter-ZN slits through the covering ZNs outmatches the rates of ion diffusion from the liquid-filled inter-ZN nanospaces back to the bulk solution. Thus, supersaturation and crystallization of dissolved salt can occur at the entrance of the inter-ZN spaces to block the liquid solution from penetrating deeply into the ZNL layer as schematically illustrated in Figure 4C.[8]

Another identically synthesized ZNL-PVDF membrane was examined by SEM and EDS survey after a 2-day PV desalination operation for the 22 wt % TDS feed solution. The membrane also exhibited an overall R_i > 99.9% and J_w > 10 kg/m^2·h, which were consistent with the other membranes been tested. The membrane was carefully retrieved from the PV cell after the feed solution was drained and subsequently dried without wiping off the remaining liquid on the ZNL surface. The EDS line-scanning results shown in Figure 4D and E revealed that the dissolved salts were blocked at the ZNL outer surface without penetrating through the ZN layer. The SEM and EDS survey over the surface of the ZNL layer and back side of the PVDF substrate further confirmed the absence of salt migration to the permeate side (Figure S5). Large-size salt crystals were observed on the ZNL surface (Figure S5a and c), but no salt was detectable by EDS on the PVDF back surface (Figure S5b and d). The very large salt crystals might have grown from the remaining solution during drying. The excellent R_i of the ZNL-PVDF also suggests that a pinhole-free ZNL layer was obtained by the filtration-coating method, which has a "self-repairing" effect as depicted in Figure S6. The results also indicate that no cracks formed during the drying/curing and rehydration cycles of membrane preparation and application processes because of the flexibility of the polymer-interlocked ZNL thin layer structure and the nonswelling nature of the PVDF.

More significantly, with the near-perfect salt rejections, the ZNL-PVDF exhibited water fluxes of 14 and 11 kg/m^2·h for the feeds with TDS of 6.77 and 22.04 wt %, respectively. These fluxes are more than 300% and 500% of those achieved by the ZNL-alumina (Figure 4B). The bare PVDF substrate, while showing far greater fluxes, was incapable of desalinating the brines. The PVDF substrate had J_w = 54 kg/m^2·h but with R_i < 18% even for the feed of 6.77% TDS (see results in Figure S7). To our knowledge, the simultaneously achieved near-perfect salt rejections, high water fluxes, and stability by the ZNL-PVDF have not been reached by any types of membrane desalination processes for such a high feed TDS. The moderate decrease of J_w by increasing feed TDS from 6.77 to 22.04 wt % was apparently caused by the reduced equilibrium vapor pressure (P_f^v) of the higher TDS solution. Increasing TDS reduces the driving force for water transport (i.e., $\Delta P_w = P_f^v - P_p^v$) that leads to decreases in J_w as predicted by eq 3. The water vapor permeance (P_m) of the ZNL-PVDF was 7.2 × 10^{-6}

https://dx.doi.org/10.1021/acsanm.1c00046
ACS Appl. Nano Mater. 2021, 4, 2895−2902

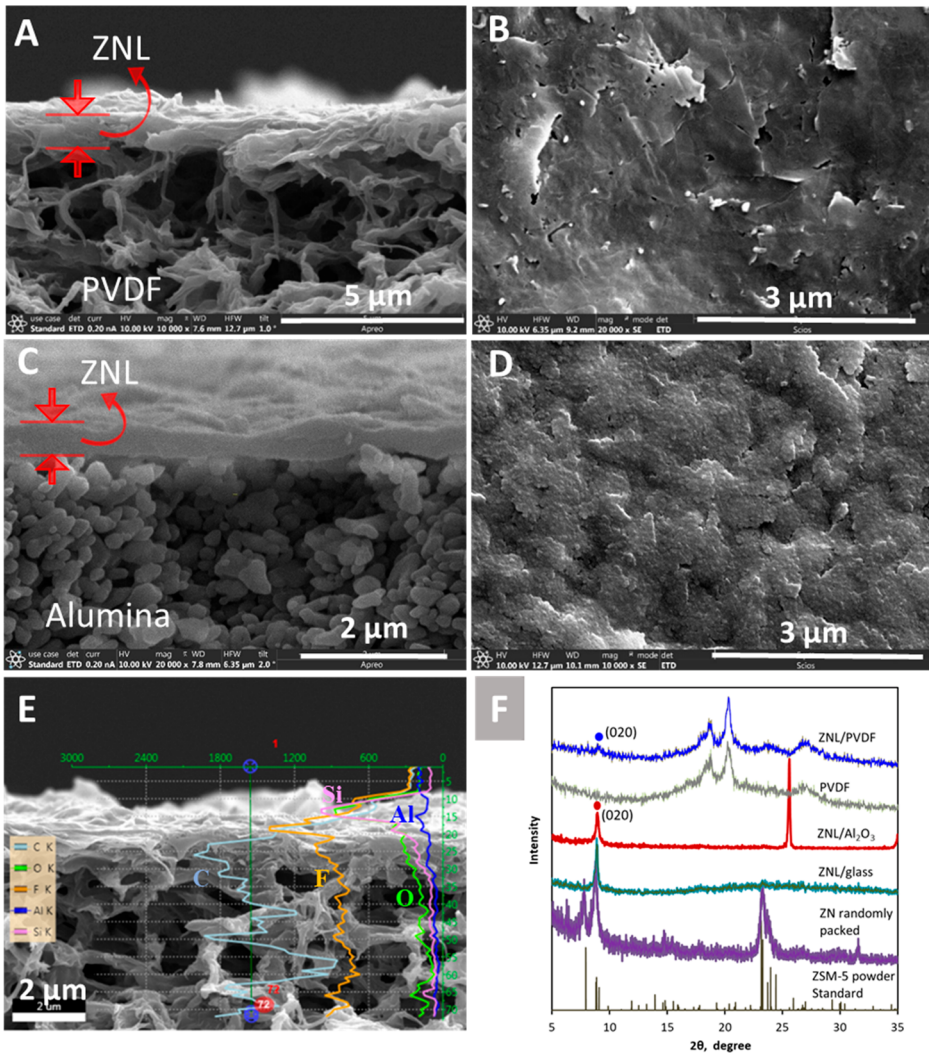

Figure 3. Characterization of the supported ZNL membranes: (A and B) cross-section and surface SEM images of ZNL-PVDF, (C and D) cross-section and surface SEM images of ZNL-alumina, (E) elemental distribution along the ZNL-PVDF membrane depth measured by EDS line-scan, and (F) XRD spectra of the randomly packed ZNs, the PVDF and alumina substrates, the supported ZNL membranes, and the ZSM-5 powder standard.[31]

and 6.0×10^{-6} mol/m^2·s·Pa for feeds of 6.77 and 22.04 wt % TDS, respectively. The reasonably consistent P_m values also indicate the avoidance of spreading salt precipitation into the inter-ZN spaces and substrate porosity for high feed TDS because blockage of the membrane pores would sensitively affect the P_m.[8]

The effect of substrate resistance $(1/P_{m,s})$ on the overall membrane J_w is described by eqs 3 and 4. From the J_w of the bare substrates, the transport resistance of the alumina disc $(1/P_{alumina})$ was estimated to be ~70 times that of the PVDF, that is, $(P_{m,PVDF}/P_{m,alumina}) \approx 70$, because the PVDF has much larger pores, greater porosity, and smaller thickness than the alumina support. However, the substrate resistance was found to impact the overall membrane P_m rather moderately for the ZNL membranes. For example, the $P_{m,z}$ of the ZNL membranes would have increased by less than 5% even if the substrates became resistance-free. Nevertheless, the substrate structural and material properties are critically important to the overall membrane performance. The porosity of the substrate and the type of bonding between the substrate and ZNL layer surfaces determine the amount of zeolite pore entrances being blocked at substrate/ZNL bonding points. For the ZNL-alumina consolidated by vapor phase-crystallization and calcination, there is more severe blockage of the zeolitic channel entrances in the alumina-supported ZNL surface. This is likely the primary cause for its significantly lower P_m, which were 1.6×10^{-6} and 0.75×10^{-6} mol/m^2·s·Pa for feeds with TDS of 6.77 and 22.04 wt %, respectively.

To further understand the PV performance of ZNL-PVDF, the vapor permeance of the ZNL layer is normalized by the substrate porosity (i.e., $P_{m,z}/\varepsilon_{substart}$) to represent the intrinsic ZNL layer properties. The porosity-normalized permeance of the apparently thicker ZNL layer on PVDF $(P_{m,z}/\varepsilon_{PVDF})$ was still 60% and 190% greater than those of the thinner ZNL layer on alumina $(P_{m,z}/\varepsilon_{alumina})$ for solution TDS values of 6.77 and 22.04 wt %, respectively. It can be inferred from the synthesis processes and results of microstructural and chemical characterizations that the ZNL layer on PVDF had polymer molecules laying sparsely between the ZNs to create inter-ZN spacing, and the alumina-supported ZNL layer contained zeolitic materials formed by vapor phase crystallization to keep spaces between ZNs. The multilayered ZNs simply consolidated by firing at high temperature without vapor phase crystallization could readily peel off from the substrate or

https://dx.doi.org/10.1021/acsanm.1c00046
ACS Appl. Nano Mater. 2021, 4, 2895−2902

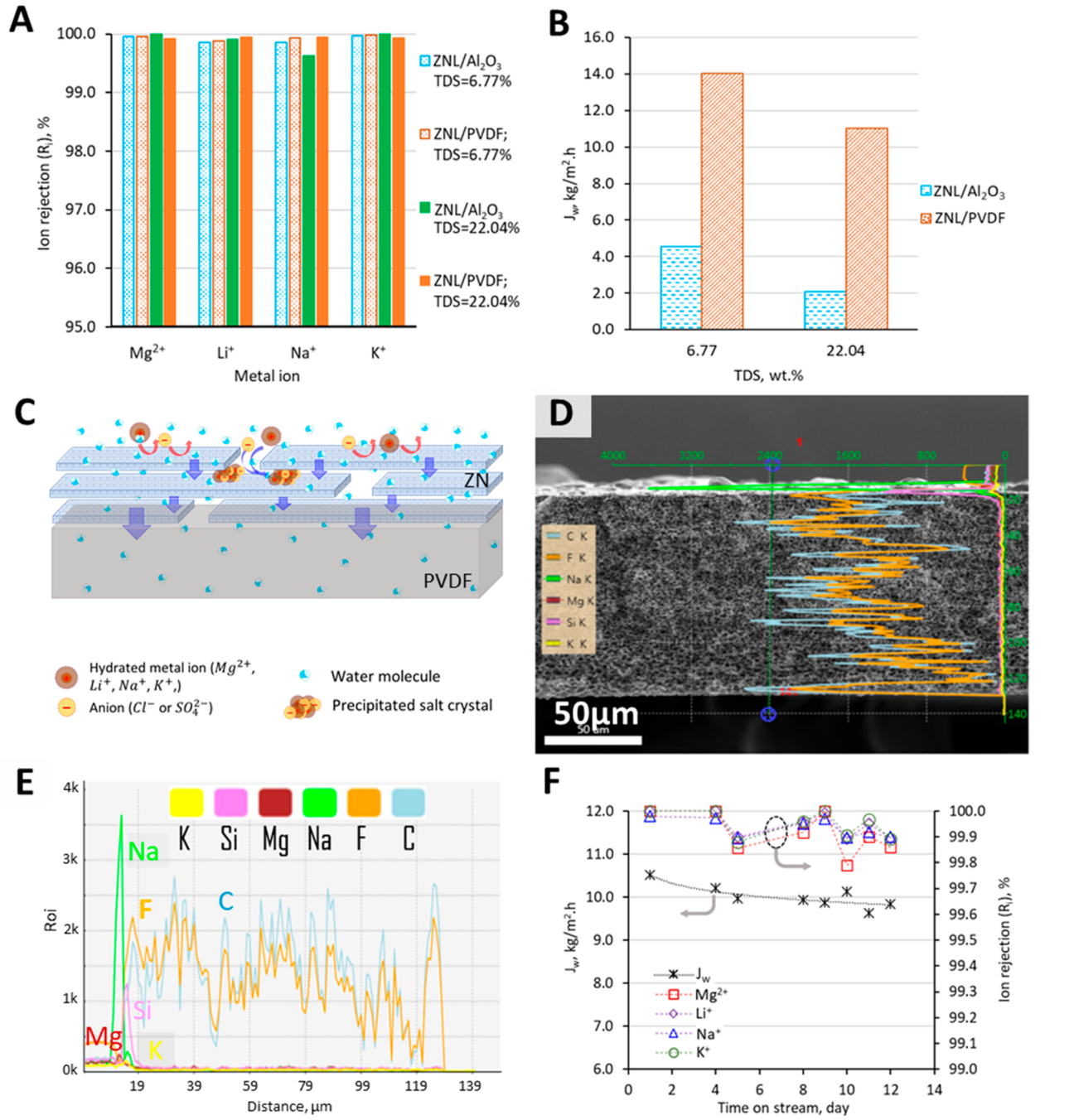

Figure 4. PV desalination for multicomponent brines at 73 °C. (A) Ion rejections on ZNL-PVDF and ZNL-alumina, (B) water fluxes of ZNL-PVDF and ZNL-alumina, (C) schematic showing salt rejection mechanisms on the ZNL membranes, (D) elemental survey by SEM-EDS line-scan across the ZNL-PVDF thickness, (E) element distributions along the entire thickness of the ZNL-PVDF, and (F) long-term PV desalination test of ZNL-PVDF using feed with TDS = 22.04 wt %.

redisperse in aqueous solutions.[8,23] In addition to the loss of zeolite pore entrances at ZN/alumina contacting points, the zeolite nanocrystals randomly grown on the surface of internal ZN layers could also hinder the water transport because of channel misalignments in these crystals. On the contrary, the nonionic PVDF molecule binders are not chemically bonded to the ZN surface, as confirmed by the FT-IR spectrum of ZNL-PVDF membrane (Figure S8). Therefore, the flexible and sparsely covered polymer chains are expected to minimally obstruct the water molecules from entering the zeolitic pores. This may explain the $P_{m,z}/\varepsilon_{PVDF}$ value being substantially greater than the $P_{m,z}/\varepsilon_{alumina}$ value. Consequently, the ZNL-PVDF allows for more efficient vapor transport through individual ZNs to faster dewater and induce salt crystallization near entrances of the inter-ZN nanospaces, although it has a more flexible structure.

The nonionic nature of the PVDF-ZN interlocked structure may also help the membrane stability by not involving solvation and dissociation of ionic bonds in aqueous solutions. The ZNL-PVDF demonstrated excellent stability in a 12-day continued PV desalination of the solution with 22.04 wt % TDS (Figure 4F). SEM survey of the ZNL-PVDF membrane

https://dx.doi.org/10.1021/acsanm.1c00046
ACS Appl. Nano Mater. 2021, 4, 2895−2902

used for the 12-day PV desalination showed no sign of ZN detachment and no noticeable changes in ZNL membrane surface morphology as compared to the fresh membrane (Figure S9).

4. CONCLUSIONS

A submicrometer-thick, *b*-oriented ZSM-5 zeolite nanosheet laminated (ZNL) membrane has been fabricated on the macroporous PVDF film substrate. The ZNL membrane layer consisted of preactivated ZSM-5 ZNs of very large aspect ratios (>100) and nanometer-scale thickness (~7.5 nm). The ZNs were interlocked by the substrate-type PVDF binder. The ZNL-PVDF membrane exhibited extraordinary water flux (>10 $kg/m^2 \cdot h$) and overall salt rejection (>99.9%) in PV desalination of high-TDS brines (22 wt %) with good stability. The enabling factors for the remarkable membrane performance in PV desalination have been discussed on the basis of the analyses of the ZNL nanostructure−property relationships. The experimental data have inferred that the fast transport of water through the individual ZN makes the solution dewatering rate surpass the ion diffusion rates in the inter-ZN nanospaces. This unique transport behavior in the ZNL causes supersaturation and crystallization of dissolved salts near entrances of the inter-ZN slits to prevent ions from migrating through the ZNL layer. The results of this work show a promising path to manufacturing high-performance ZNL membranes on practically meaningful polymer supports for tackling the growing challenges in treating and reusing many industrially produced high-TDS wastewaters.

■ ASSOCIATED CONTENT

Supporting Information

The Supporting Information is available free of charge at https://pubs.acs.org/doi/10.1021/acsanm.1c00046.

Methods for syntheses of dC5 SDA and ZSM-5 nanosheets and preparation of preactivated ZN suspensions, procedure for fabricating the ZSM-5 ZNL-alumina membrane, specifications of chemicals and materials employed in this study, derivation of "lumped permeability" of the ZNL layer, graphic illustrations of the MFI zeolitic channel system, SEM pictures of the porous PVDF before and after contacting the EtOH/DMSO mixed solvents, zeta potential of ZNs in aqueous solutions, SEM and EDS survey of the ZNL layer and PVDF substrate surfaces after 2 days of PV desalination for 22% TDS solution, schematic diagram of the membrane PV desalination apparatus, cross-sectional SEM pictures of ZNL layers formed without PVDF binder or without consolidation by vapor phase crystallization, illustration of the "self-repairing" effect in the vacuum-filtration coating process, results of PV desalination on bare PVDF film, FT-IR spectra of the ZNL-PVDF membrane and components, and a summary of reports on desalination by zeolite-based membranes (PDF)

■ AUTHOR INFORMATION

Corresponding Author

Junhang Dong − *Department of Chemical and Environmental Engineering, University of Cincinnati, Cincinnati, Ohio 45221, United States;* orcid.org/0000-0002-4393-4968; Email: junhang.dong@uc.edu

Authors

Zishu Cao − *Department of Chemical and Environmental Engineering, University of Cincinnati, Cincinnati, Ohio 45221, United States*

Landysh Iskhakova − *Department of Chemical and Environmental Engineering, University of Cincinnati, Cincinnati, Ohio 45221, United States*

Xinhui Sun − *Department of Chemical and Environmental Engineering, University of Cincinnati, Cincinnati, Ohio 45221, United States*

Zhong Tang − *Bettergy Corporation, Peekskill, New York 10566, United States*

Complete contact information is available at: https://pubs.acs.org/10.1021/acsanm.1c00046

Notes

The authors declare no competing financial interest.

■ ACKNOWLEDGMENTS

This research was supported by the U.S. National Science Foundation (grant no. CBET-1935205) and the U.S. Department of Energy (grant no. DE-SC0020011). We thank Professor A. Angelopoulos for help with zeta-potential measurements.

■ REFERENCES

(1) Choi, M.; Na, K.; Kim, J.; Sakamoto, Y.; Terasaki, O.; Ryoo, R. Stable single-unit-cell nanosheets of zeolite MFI as active and long-lived catalysts. *Nature* **2009**, *461*, 246−249.

(2) Liu, G.; Jin, W.; Xu, N. Two-Dimensional-Material Membranes: A New Family of High-Performance Separation Membranes. *Angew. Chem., Int. Ed.* **2016**, *55*, 13384−13397.

(3) Ma, X. L.; Kumar, P.; Mittal, N.; Khlyustova, A.; Daoutidis, P.; Mkhoyan, K. A.; Tsapatsis, M. Zeolitic imidazolate framework membranes made by ligand-induced permselectivation. *Science* **2018**, *361*, 1008−1011.

(4) Sint, K.; Wang, B.; Král, P. Selective Ion Passage through Functionalized Graphene Nanopores. *J. Am. Chem. Soc.* **2008**, *130*, 16448−16449.

(5) Varoon, K.; Zhang, X.; Elyassi, B.; Brewer, D. D.; Gettel, M.; Kumar, S.; Lee, J. A.; Maheshwari, S.; Mittal, A.; Sung, C. Y.; Cococcioni, M.; Francis, L. F.; McCormick, A. V.; Mkhoyan, K. A.; Tsapatsis, M. Dispersible exfoliated zeolite nanosheets and their application as a selective membrane. *Science* **2011**, *334*, 72−75.

(6) Yuan, S.; Li, Y.; Xia, Y.; Kang, Y.; Yang, J.; Uddin, M. H.; Liu, H.; Selomulya, C.; Zhang, X. Environ. Minimizing Non-selective Nanowrinkles of Reduced Graphene Oxide Laminar Membranes for Enhanced NaCl Rejection. *Environ. Sci. Technol. Lett.* **2020**, *7*, 273−279.

(7) Hirunpinyopas, W.; Prestat, E.; Worrall, S. D.; Haigh, S. J.; Dryfe, R. A. W.; Bissett, M. A. Desalination and Nanofiltration through Functionalized Laminar MoS2Membranes. *ACS Nano* **2017**, *11*, 11082−11090.

(8) Cao, Z.; Zeng, S.; Xu, Z.; Arvanitis, A.; Yang, S.; Gu, X.; Dong, J. Ultrathin ZSM-5 Zeolite Nanosheet Laminated Membrane for High-Flux Desalination of Concentrated Brines. *Sci. Adv.* **2018**, *4*, No. eaau8634.

(9) Hoenig, E.; Strong, S. E.; Wang, M.; Radhakrishnan, J. M.; Zaluzec, N. J.; Skinner, J. L.; Liu, C. Controlling the Structure of MoS2Membranes via Covalent Functionalization with Molecular Spacers. *Nano Lett.* **2020**, *20*, 7844−7851.

(10) Lai, Z.; Bonilla, G.; Diaz, I.; Nery, J. G.; Sujaoti, K.; Amat, M. A.; Kokkoli, E.; Terasaki, O.; Thompson, R. W.; Tsapatsis, M.; Vlachos, D. G. Microstructural optimization of a zeolite membrane for organic vapor separation. *Science* **2003**, *300*, 456−460.

(11) Li, L.; Dong, J.; Nenoff, T. M.; Lee, R. Desalination by reverse osmosis using MFI zeolite membranes. *J. Membr. Sci.* **2004**, *243*, 401−404.
(12) Yang, R.; Xu, Z.; Yang, S.; Li, L.; Angelopoulos, A.; Dong, J. Nonionic zeolite membrane as potential ion separator in redox-flow battery. *J. Membr. Sci.* **2014**, *450*, 12−17.
(13) Jamali, S. H.; Vlugt, T. J. H.; Lin, L. C. Atomistic understanding of zeolite nanosheets for water desalination. *J. Phys. Chem. C* **2017**, *121*, 11273−11280.
(14) Chen, X.; Yip, N. Y. Unlocking high-salinity desalination with cascading osmotically mediated reverse osmosis: energy and operating pressure analysis. *Environ. Sci. Technol.* **2018**, *52*, 2242−2250.
(15) Yang, Z.; Ma, X. H.; Tang, C. Y. Recent development of novel membranes for desalination. *Desalination* **2018**, *434*, 37−59.
(16) Goh, P. S.; Ismail, A. F. A review on inorganic membranes for desalination and wastewater treatment. *Desalination* **2018**, *434*, 60−80.
(17) Darwish, M. A.; Al-Juwayhel, F.; Abdulraheim, H. K. Multi-effect boiling systems from an energy viewpoint. *Desalination* **2006**, *194*, 22−39.
(18) Kaplan, R.; Mamrosh, D.; Salih, H. H.; Dastgheib, S. A. Assessment of desalination technologies for treatment of a highly saline brine from a potential CO_2 storage site. *Desalination* **2017**, *404*, 87−101.
(19) Jeon, M. Y.; Kim, D.; Kumar, P.; Lee, P. S.; Rangnekar, N.; Bai, P.; Shete, M.; Elyassi, B.; Lee, H. S.; Narasimharao, K.; Basahel, S. N.; Al-Thabaiti, S.; Xu, W.; Cho, H. J.; Fetisov, E. O.; Thyagarajan, R.; DeJaco, R. F.; Fan, W.; Mkhoyan, K. A.; Siepmann, J. I.; Tsapatsis, M. Ultra-selective high-flux membranes from directly synthesized zeolite nanosheets. *Nature* **2017**, *543*, 690−694.
(20) Kim, D.; Jeon, Y.; Stottrup, B. L.; Tsapatsis, M. Para-xylene ultra-selective zeolite MFI membranes fabricated from nanosheet monolayers at the air-water interface. *Angew. Chem., Int. Ed.* **2018**, *57*, 480−485.
(21) Min, B.; Yang, S.; Korde, A.; Kwon, Y. H.; Jones, C. W.; Nair, S. Continuous zeolite MFI membranes fabricated from 2D MFI nanosheets on ceramic hollow fibers. *Angew. Chem., Int. Ed.* **2019**, *58*, 8201−8205.
(22) Dong, J.; Lin, Y. S.; Hu, M. Z. C.; Peascoe, R. A.; Payzant, E. A. Template removal associated microstructural development of ceramic supported MFI zeolite membranes. *Microporous Mesoporous Mater.* **2000**, *34*, 241−253.
(23) Zhang, H.; Xiao, Q.; Guo, X.; Li, N.; Kumar, P.; Rangnekar, N.; Al-Thabaiti, S.; Jeon, M. Y.; Narasimharao, K.; Basahel, S. N.; Topuz, B.; Onorato, F. J.; Macosko, C. W.; Mkhoyan, K. A.; Tsapatsis, M. Open-pore two-dimensional MFI zeolite nanosheets for the fabrication of hydrocarbon-isomer-selective membranes on porous polymer supports. *Angew. Chem., Int. Ed.* **2016**, *55*, 7184−7187.
(24) Li, L.; Dong, J.; Nenoff, T. M.; Lee, R. Reverse osmosis of ionic aqueous solutions on a MFI zeolite membrane. *Desalination* **2004**, *170*, 309−316.
(25) Li, L.; Liu, N.; McPherson, B.; Lee, R. Enhanced water permeation of reverse osmosis through MFI-type zeolite membranes with high aluminum contents. *Ind. Eng. Chem. Res.* **2007**, *46*, 1584−1589.
(26) Özgür Yazaydın, A.; Thompson, R. W. Molecular simulation of water adsorption in silicalite: effect of silanol groups and different cations. *Microporous Mesoporous Mater.* **2009**, *123*, 169−176.
(27) Drobek, M.; Yacou, C.; Motuzas, J.; Julbe, A.; Ding, L.; Diniz da Costa, J. C. Long term pervaporation desalination of tubular MFI zeolite membranes. *J. Membr. Sci.* **2012**, *415−416*, 816−823.
(28) Xu, Z.; Michos, I.; Cao, Z.; Jing, W.; Gu, X.; Kinkel, K. R.; Murad, S.; Dong, J. Proton-selective ion transport in ZSM-5 zeolite membrane. *J. Phys. Chem. C* **2016**, *120*, 26386−26392.
(29) Duke, M. C.; O'Brien-Abraham, J.; Milne, N.; Zhu, B.; Lin, Y. S.; Diniz da Costa, J. C. Seawater desalination performance of MFI type membranes made by secondary growth. *Sep. Purif. Technol.* **2009**, *68*, 343−350.
(30) Jakli, G.; van Hook, W. A. The Vapor Pressures of Dimethyl Sulfoxide and Hexadeuterodimethyl Sulfoxide from about 313 to 453 K. *J. Chem. Thermodyn.* **1972**, *4* (6), 857−864.
(31) Baerlocher, C., McCusker, L. B., Olson, D. H., Eds. *Atlas of Zeolite Framework Types*, 7th ed.; Structure Commission of the International Zeolite Association, Elsevier: Oxford, UK, 2007.
(32) Cha-Umpong, W.; Li, Q.; Razmjou, A.; Chen, V. Concentrating brine for lithium recovery using GO composite pervaporation membranes. *Desalination* **2021**, *500*, 114894.
(33) Li, L.; Dong, J.; Nenoff, T. M. Transport of alkaline metal ions in MFI zeolite membranes during reverse osmosis. *Sep. Purif. Technol.* **2007**, *53*, 42−48.
(34) Kazemimoghadam, M.; Mohammadi, T. Synthesis of MFI zeolite membranes for water desalination. *Desalination* **2007**, *206*, 547−553.
(35) Liu, X.; Demir, N. K.; Wu, Z.; Kang Li, K. Highly Water-Stable Zirconium Metal-Organic Framework UiO-66 Membranes Supported on Alumina Hollow Fibers for Desalination. *J. Am. Chem. Soc.* **2015**, *137*, 6999−7002.
(36) Marcus, Y. Concentration dependence of ionic hydration numbers. *J. Phys. Chem. B* **2014**, *118*, 10471−10476.
(37) Nagasaka, M.; Yuzawa, H.; Kosugi, N. Interaction between water and alkali metal ions and its temperature dependence revealed by oxygen K-edge X-ray absorption spectroscopy. *J. Phys. Chem. B* **2017**, *121*, 10957−10964.

https://dx.doi.org/10.1021/acsanm.1c00046
ACS Appl. Nano Mater. 2021, 4, 2895−2902